## Title

Revealing Ligand Binding Sites and Quantifying Subunit Variants of Noncovalent Protein Complexes in a Single Native Top-Down FTICR MS Experiment



## Journal

Journal of The American Society for Mass Spectrometry, 25(12)

## ISSN

1044-0305

## Authors

Li, Huilin
Wongkongkathep, Piriya
Van Orden, Steve L
et al.

## Publication Date

2014-12-01

## DOI

10.1007/s13361-014-0928-6

Peer reviewed

HHS Public Access

Author manuscript

*J Am Soc Mass Spectrom*. Author manuscript; available in PMC 2015 May 26.

Published in final edited form as:

*J Am Soc Mass Spectrom*. 2014 December ; 25(12): 2060–2068. doi:10.1007/s13361-014-0928-6.

# Revealing Ligand Binding Sites and Quantifying Subunit Variants of Non-Covalent Protein Complexes in a Single Native Top-Down FTICR MS Experiment

**Huilin Li**[†], **Piriya Wongkongkathep**[#], **Steve L. Van Orden**[@], **Rachel R. Ogorzalek Loo**[†], and **Joseph A. Loo**[†,#,*]

[†] Department of Biological Chemistry, David Geffen School of Medicine at UCLA, University of California, Los Angeles, CA, 90095, USA

[#] Department of Chemistry and Biochemistry, University of California, Los Angeles, CA, 90095, USA

[@] Bruker Daltonics, 40 Manning Road, Billerica, MA, 01821, USA

## Abstract

"Native" mass spectrometry (MS) has been proven increasingly useful for structural biology studies of macromolecular assemblies. Using horse liver alcohol dehydrogenase (hADH) and yeast alcohol dehydrogenase (yADH) as examples, we demonstrate that rich information can be obtained in a single native top-down MS experiment using Fourier transform ion cyclotron mass spectrometry (FTICR MS). Beyond measuring the molecular weights of the protein complexes, isotopic mass resolution was achieved for yeast ADH tetramer (147 kDa) with an average resolving power of 412,700 at *m/z* 5466 in absorption mode and the mass reflects that each subunit binds to two zinc atoms. The N-terminal 89 amino acid residues were sequenced in a top-down electron capture dissociation (ECD) experiment, along with the identifications of the zinc binding site at Cys46 and a point mutation (V58T). With the combination of various activation/dissociation techniques, including ECD, in-source dissociation (ISD), collisionally activated dissociation (CAD), and infrared multiphoton dissociation (IRMPD), 40% of the yADH sequence was derived directly from the native tetramer complex. For hADH, native top-down ECD-MS shows that both E and S subunits are present in the hADH sample, with a relative ratio of 4:1. Native top-down ISD MS hADH dimer shows that each subunit (E and S chain) binds not only to two zinc atoms, but also the $NAD^+$/NADH ligand, with a higher $NAD^+$/NADH binding preference for the S chain relative to the E chain. In total, 32% sequence coverage was achieved for both E and S chains.

## INTRODUCTION

Studying how proteins interact with one another and assemble on a structural basis is key to understanding biological processes and their function. As a complementary technique to conventional technologies used in structural biology, such as nuclear magnetic resonance

[*] *Correspondence to:* Joseph A. Loo; JLoo@chem.ucla.edu.

(NMR) spectroscopy, X-ray crystallography, and electron microscopy, “native” mass spectrometry (MS) has established its crucial role in the characterization of intact noncovalently-bound protein complexes, revealing the composition, stoichiometry, dynamics, stability, and also spatial information of subunit arrangements in protein assemblies [1-11]. To date, most native MS studies of protein complexes have been performed using quadrupole time-of-flight (Q-TOF) MS instruments with electrospray ionization (ESI). Because of the efficient transmission of high mass and high*m/z* ions using TOF analyzers, large proteins with molecular weights up to 18 MDa have been studied [12, 13]. The coupling of ion mobility spectrometry (IMS) with mass spectrometry provides a new dimension to the analysis of biomolecules [14]. With IMS, ions are separated based on size and shape, and the IMS-derived collision cross-section information can be used to understand the topological properties of gas phase protein complexes. Surface induced dissociation (SID) has been recently added for the purposes of disassembling protein complexes into sub-complexes that appear to better reflect the structure of the solution phase complexes [15-17]. The capability of Orbitrap MS has been extended significantly for the analysis of macromolecules, with greatly improved mass (and *m/z*) range and resolving power to measure the binding of ADP and ATP to the 800 kDa GroEL complex [18].

Fourier transform ion cyclotron resonance mass spectrometry (FTICR MS) is known for its superior resolving power and mass accuracy and its capabilities for tandem MS (MS/MS) with a variety of fragmentation techniques. Particularly, after the introduction of electron capture dissociation (ECD) [19], FTICR MS quickly established its utility for protein top-down protein sequencing, post-translational modification characterization, and protein gas phase studies [20-34]. Polypeptide backbone bonds are cleaved by ECD, but non-covalent interactions are preserved, which therefore makes the native top-down MS study of the non-covalent interaction sites of protein-ligands complexes more feasible. Our group and others have successfully applied top-down ECD-MS to pinpoint the interaction sites of several protein-ligand system [35-38], and this can be enhanced by “supercharging” [35]. An early attempt of applying ECD-MS to the study of large protein complexes was made by Heeren and Heck, but little topology and sequence information was derived [39]. However, the Gross group starting in 2010 made the first breakthrough for the study of large protein complexes using native top-down ECD with FTICR MS. Besides obtaining molecular weight, sequence, and metal-binding site information in a single MS experiment, they correlated the origins of ECD product ions to the flexible regions of proteins as determined by the “B-factor” from the X-ray crystal structures of protein complexes [40, 41]. Therefore, native top-down ECD has been proposed as a tool to probe the flexible regions of protein complexes. Our group recently also demonstrated the capability of obtaining sequence information *and* isotopic mass resolution of a noncovalently-bound protein complex of 158 kDa using native top-down FTICR MS, and most importantly, we found that the origin of ECD fragments is not limited only to the flexible region of the protein complex (e.g., tetrameric aldolase), but also largely from the *surface* of the complex [42].

The application of FTICR MS for native top-down interrogation of large non-covalent bound protein complexes is still in its infancy. Here, for the purpose of further exploring the capability of FTICR MS in the analysis of large protein complexes, various fragmentation

techniques including in-source dissociation (ISD), collisionally activated dissociation (CAD), ECD, and infrared multiphoton dissociation (IRMPD) were applied in the native top-down MS studies of a 80 kDa dimeric protein complex and a 147 kDa tetrameric protein complex. The results demonstrate that with the superior resolving power, mass accuracy, and versatile fragmentation techniques of FTICR MS, rich information, including isotopic mass resolution, amino acid sequence, point mutations, metal/ligand binding sites, and identification and quantification of subunit variants can be accomplished in a single native top-down FTICR MS experiment.

## EXPERIMENTAL

### Materials

Alcohol dehydrogenases (ADH) from yeast and horse liver and ammonium acetate were purchased from Sigma-Aldrich (St. Louis, MO). Acetonitrile and formic acid were obtained from Fisher Scientific (Pittsburgh, PA).

### Sample Preparation

Yeast and horse liver ADH were dissolved in MilliQ water to a concentration of 100 μM, and then buffer exchanged three times with 200 mM ammonium acetate solution (300 μL each time) using Amicon centrifugal filters (Millipore Inc., Billerica, MA) with a molecular weight cut-off (MWCO) of 50 K. The buffer exchanged protein samples were then diluted with 200 mM ammonium acetate solution to a concentration of 20 μM for native nano-ESI-MS analysis.

### FTICR MS Analysis

Protein solutions were loaded into metal-coated borosilicate capillaries (Au/Pd-coated, 1 μm I.D.; Thermo Fisher Scientific, West Palm Beach, FL) and sprayed at a flow rate of 10 - 40 nL/min through a nanospray ion source. The experiments were performed using a 15-T Bruker SolariX FTICR MS with an infinity cell. The ESI capillary voltage was set to 0.9~1.2 kV. The temperature of dry gas was 80 ºC and the flow rate was 2.5 L/min. The RF amplitude of the ion-funnels was 300 $V_{pp}$, and the applied voltages were 210 V and 6 V for funnels 1 and 2, respectively. The voltage of skimmer 1 was varied up to 200 V to pre-heat ions but without inducing fragmentation and the skimmer 2 voltage was kept at 20 V. The lowest values of RF frequencies were used in all ion-transmission regions: multipole 1 (2 MHz), quadrupole (1.4 MHz), and transfer hexapole (1 MHz). Ions were accumulated for 500 ms in the hexapole collision cell before being transmitted to the infinity ICR cell. The time-of-flight of 2.5 ms was used. Vacuum pressures for different regions were ~2 mbar for the source region, ~$2\times10^{-6}$ mbar for the quadrupole region, and ~$2\times10^{-9}$ mbar for the UHV-chamber pressure. ECD experiments were performed with an ECD pulse length of 0.02 s, ECD bias of 1.5 V, and ECD lens of 15 V. The ECD hollow-cathode current was 1.6 A. IRMPD was performed with a Synrad 30-W $CO_2$ laser (Mukilteo, WA) that was interfaced to the back of the mass spectrometer. The laser power was varied up to 80% (30 W) for all IRMPD experiments, and the irradiation time was kept at 0.5 s. Up to 300 scans were averaged for each spectrum and all spectra were externally calibrated with cesium iodide. Data was processed in DataAnalysis (Bruker) and interpreted manually. Peaks were detected

using the SNAP centroid peak detection algorithm (version 2.0) with quality factor threshold of 0.5, signal-to-noise threshold of 2, and maximum charge state of 40. The phase correction of the yeast ADH tetramer complex was done with the Bruker solariX™ XR software.

## RESULTS AND DISSCUSSION

Alcohol dehydrogenase is present in many organisms and catalyzes the oxidation of alcohols with the reduction of $NAD^+$ to NADH. Horse liver alcohol dehydrogenase (hADH) and yeast alcohol dehydrogenase (yADH) are distantly related, but have different quaternary structures and subunit sizes. yADH is a homotetrameric protein with a total molecular weight of 147 kDa (~ 36 kDa for each subunit), whereas hADH is a dimeric protein of ~ 80 kDa with three main isoenzymes, which are the combinations of two different types of subunits (~ 40 kDa for each subunit; EE, SS, and ES, where E stands for “ethanol-active” and S for “steroid-active”).

### Native Top-Down ECD, ISD, and IRMPD of Horse Liver ADH

Subunits E (UniProt: P00327) and S (UniProt: P00328) are highly identical in sequence with differences of only 9 amino acids out of 374. Each subunit binds a molecule of $NAD^+$, a zinc at the active site, and an additional zinc that is structural. The zinc at the active site coordinates to Cys46, His67, Cys174 (Cys173 for subunit S), and one water molecule. The other zinc binds to Cys97, Cys100, Cys103, and Cys111.

The inset of Figure 1A (left-hand side) shows the native nano-ESI mass spectrum of hADH. Ions for the hADH dimer appear at *m/z* 3500–4500 with charge states of 23+ to 20+, along with nonspecific hADH tetramers present in the higher *m/z* region. The peak width of each charge state corresponds to about ~100 Da, indicating sample heterogeneity and ligand/cation/solvent/buffer adduction. The entire charge state envelope of hADH was subjected to top-down ECD fragmentation and the ECD spectrum is shown in Figure 1A. Fragments from both E and S chains were observed in the top-down ECD mass spectrum of hADH, with the fragmentation map shown on the right-hand side of Figure 1A. Counting from the N-terminus, the first sequence difference between the E chain and S chain is at residue 17 (Glu17 vs Gln17), which is a mass difference of 0.9840 Da. Figure 1B shows the expanded spectra of product ions of hADH. The mass difference (Δm) between $c_{16}^{2+}$ at *m/z* 872.99270 and the doubly charged ions at *m/z* 937.51392 is 129.04244 Da, which matches the sequence of subunit E with Glu17. Similarly, the Δm between $c_{16}^{2+}$ and the doubly charged ions at *m/z* 937.02191 is 128.05842 Da, corresponding to Gln17 of subunit S. To clarify the annotation for ions from different subunits, the c-product ions from subunit E and subunit S are, for example, annotated as $^{E}c_{17}^{2+}$ (in black) and $^{s}c_{17}^{+}$ (in red), respectively. All ions were assigned with sub-ppm mass accuracy; in addition, the expanded spectrum of ions at *m/z* 937.5 (right side of Figure 1B) shows both the isotopic A ion of $^{E}c_{17}^{2+}$ and the isotopic A+1 ion of $^{E}c_{17}^{2+}$, proving the presence of both subunits. Figure 1C presents the second sequence difference between subunits E and S at residue 44 (Thr vs Ala). Overall, the first 89 amino acids from the N-termini of the sequences were identified. Beyond subunit differentiation and sequencing, a series of c-ions from subunit E bound to zinc were also observed, starting from $(c_{50}+Zn)^{4+}$. The $(c_{53}+Zn)^{4+}$ ion is shown in Figure 1D, which has a wilder isotopic distribution compared to regular c-ions due to the contribution of the zinc

isotopes. The observation of $(c_{50}+Zn)^{4+}$ ions is consistent with the known zinc binding position at the active site, Cys46.

Besides the characterization of subunits E and S, two additional subunits with similar sequences to subunit E and subunit S but with a putative PTM at the N-terminal region were found. According to the sequence similarity of the two unknown subunits to subunits E or S, one of them is denoted as subunit *E and the other as subunit *S. The sequence difference between subunit E and subunit *E is found at the N-terminal region, and the same was found for subunits S and *S. As shown in Figure 1E, the mass difference between $^{E}c_{18}^{2+}$ and $^{*}Ec_{18}^{2}$ is 44.01442 Da, which corresponds to an elemental composition of $CH_2ON$ (44.01364 Da) (and the same for $^{S}c_{18}^{2+}$ and $^{*S}c_{18}^{2+}$). (The sites with the -44.01364 Da mass shifts are indicated with an asterisk at the upright shoulder of the corresponding residue letters in the fragmentation map in Figure 1A.) It can be seen that this mass shift was observed along the sequences of both E and S chains, and the first site with this putative modification starts from residue 6. The mass errors of all assigned fragment ions are plotted against the mass-to-charge ratio (Figure 2), and it can be seen that the mass errors are mostly within 3 ppm, with a few over 3 ppm but less than 5 ppm due to peak distortions caused by low signal-to-noise level. Even lower mass errors were achieved for subunit *E (blue) with < 2 ppm and subunit *S (yellow) with < 1 ppm, which further confirms that the elemental composition of the -44.01364 Da mass shift corresponds to $CH_2ON$.

Figure 1F shows the normalized abundances of c-ion products from each subunit plotted against the hADH sequences. Because the initial N-terminal 16 residues of subunits E and S are the same and cannot be differentiated by mass, the normalized abundances for each of the observed c-ions for the 16 amino acids are then equally divided into two, which does not represent the actual intensities of each ion from the different chains. The same treatment was used for subunits *E and *S. The normalized product ion abundances from subunits E and S can then be plotted to determine the ratio of the subunits present in the hADH sample, which is about ~ 4:1 E:S.

In-source dissociation, analogous to the “nozzle-skimmer” dissociation originally demonstrated by the Smith group in the early days of ESI-MS [43, 44], was achieved with the FTICR MS system by elevating skimmer 1 voltage (up to 190 V) to fragment the hADH dimer complexes, as shown in Figure 3A. Along with the dissociation of the hADH dimer to monomers, two large fragments originating from backbone cleavages with molecular weight of 13.8 and 29.4 kDa, respectively, were also observed. The 7+ charge state of the 13.8 kDa fragment ions was isolated and further fragmented by both CAD and ECD. However, only a complementary pair of ions ($m/z$ $1958^{5+}$ / $m/z$ $2030^{2+}$) was observed by CAD and no products were observed by ECD, which is primarily due to the low signal intensity of the precursor ions. To improve the peak assignment accuracy of the monomers, the 11+ charge state at $m/z$ 3635 was mass selected with a mass window of ±50 Da in the quadrupole Q1 region of the instrument and then transferred to the infinity ICR cell. A 4.6 s transient was recorded, which leads to the isotopic mass resolution of the 11+ charge state ions of the monomers at $m/z$ 3635±50 Da (see the inset of Figure 3A). The binding of two zinc atoms, $NAD^+$, or both to either E or S chains were both found. All peaks were assigned with a mass error of 3 ppm. It is interesting to notice that the S chain has an apparent higher binding

affinity to $NAD^+$ than the E chain (inset of Figure 3A); the differences in coenzyme binding between the EE and SS isoenzymes were reported in 1970 [45, 46].

Native top-down IRMPD MS was also performed for the hADH complexes without mass selection (Figure 3B). Compared to ISD, IRMPD of the hADH dimer results in more backbone cleavage fragments. In total, 39 backbone cleavages for subunit E and 26 for subunit S were observed in the IRMPD experiment, which leads to the sequencing of the first 87 residues of the N-terminal regions of both E and S chains, along with 34 residues from the C-terminal of the E chain and 31 amino acids of the S chain (inset of Figure 3B). It is worth noting that 52% of the cleavage sites for the E chain and 42% for the S chain are from preferential CAD cleavage sites, such as N-terminal proline, C-teriminal aspartic acid, and glutamic acid [47-49]. With the combination of top-down ISD, IRMPD, and ECD fragmentation techniques, an overall sequence coverage of 32% was achieved from the native hADH dimer.

## Native Top-Down ECD, ISD, CAD, and IRMPD of Yeast ADH

Yeast ADH is a homotetrameric protein with a total molecular weight of ~147 kDa. Previously it was studied by Gross and coworkers using native top-down ECD-MS with a 12-T FTICR MS; sequencing of the first 55 amino acids was reported [40]. Here, for a comparison with hADH, native top-down ECD of yADH tetramer with our experimental system was also performed. With skimmer voltage of 100 V for in-source dissociation of the yADH tetramer complex, sequencing of the first 55 residues from the N-terminus was achieved. Further increasing the skimmer voltage to 150 V yielded higher sequence coverage, with sequence information for the N-terminal 79 residues. When the skimmer 1 potential was elevated to 200 V, it not only improved the sequence coverage to the first 89 residues (Figures 4A and B) with 74 out of 88 backbone N-Cα bonds cleaved, it also releases zinc-bound fragments, e.g., $c_{49}$+Zn ~ $c_{77}$+Zn, as shown in Figures 4A and C. In addition, a site mutation at residue 58 was observed as a Thr rather than Val (Figure 4D) [50]. Moreover, the putative PTM (-44.0136 Da mass shift) observed in hADH was also found in the yADH sample, as shown in Figures 4A and D. The 44.0136 Da loss has been previously observed by ECD or ETD followed by collisional activation of peptides, resulting in side chain loss of (■$CONH_2$) from an Asn (N) or Gln (Q) residue [51, 52]. However, in both cases, the loss of ■$CONH_2$ is initiated by radical migration from z• ions to the side chain of Asn or Gln residues rather than from c ions. In addition, the loss of ■$CONH_2$ happens less frequently unless with collisional activation. Here, the -44.0136 Da mass shifts were observed along the sequences on c ions rather than z• ions. In addition, the first site observed with the -44.0136 Da mass shift is at residue 6 for horse liver ADH, but there is no N/Q in both E and S subunits before residue 17 for hADH. Therefore, we believe that the -44.0136 Da ($CONH_2$) mass shift is suggestive of a PTM or sequence modification rather than a side chain loss.

Native top-down ISD, CAD, and IRMPD were also performed on the hADH tetramer. Skimmer 1 potential was varied from 30 to 200 V, which only leads to the dissociation of the ADH tetramer to the dimer subcomplex (17+ to 21+). As skimmer 1 was kept at 200 V, further CAD activation in the collision cell and IRMPD in the infinity cell without prior

mass isolation were performed, e.g., pre-activation by increasing the skimmer potential; b/y-product ions were observed in both CAD (Figure 5A) and IRMPD (Figure 5B) experiments. In comparison, a zinc bound ion $(b_{86}+Zn)^{6+}$ and a large fragment (10.9 kDa) at *m/z* greater than 10,000 were observed in the IRMPD but not in the CAD experiment. The backbone cleavage sites at different CAD collisional voltages (labeled in black) were summarized and combined with the top-down IRMPD (yellow) and ECD (c ions in red and c+Zn ions in blue), as shown in Figure 5C. From the combination of native top-down CAD, IRMPD, and ECD results, the first 115 residues from the N-terminal and the first 25 residues from the C-terminal were sequenced, which results in 40% sequence coverage.

Comparing the full mass spectra of yADH (inset of Figure 4A) and hADH (inset of Figure 1A), the yeast ADH sample appears much cleaner, which might due to less apparent heterogeneity. An attempt to achieve isotopic mass resolution of yeast ADH tetramer was made using our infinity ICR cell. The 27+ charge state ions at *m/z* 5460±50 (Figure 6A) was isolated in the quadrupole to minimize space charge effects due to ion cloud interactions in the infinity cell. Four isotopic "beats" were observed over a recording time of 11 s (Figure 6B), which leads to isotopic resolution of the 27+ yADH tetramer with an average resolving power of ~412,000 in absorption mode (Figure 6C). With knowledge of the yeast ADH sequence, the isotopic distribution of the 27+ ions was then simulated to fit the experimental result (Figures 6A and C). It is interesting to note that each yADH subunit binds to two zinc atoms, but no $NAD^+$ binding was observed. This might reflect the fact that yADH has lower binding affinity for $NAD^+$ than hADH does, differing by up to 1 or 2 orders of magnitude at pH 8 [53, 54].

The correlation between native top-down fragmentation sites and the X-ray B-factor was examined for both ADH (yeast and horse liver) protein complexes [55, 56]. It is clear that the native top-down cleavage sites are correlated with the X-ray B-factor in both cases (Supplementary Figure 1). However, in addition, the IRMPD cleavage sites originate from both flexible (overlapping with ECD cleavage regions) and surface regions for both protein complexes.

## CONCLUSIONS

In this study, using the hADH dimer and yADH tetramer as examples, we demonstrate that with superior high resolving power, mass accuracy, and the versatile and complementary fragmentation techniques available with FTICR MS, rich information including amino acid sequence, point mutations, metal/ligand binding sites, and identification and quantification of subunit variants can be accomplished in a single native top-down FTICR MS experiment. Unlike data derived from native tandem MS using more commonly employed Q-TOF analyzers, significant sequence information can be gained *directly* from the intact noncovalently-bound complex with FTICR MS. Somewhat surprising is that CAD and IRMPD of the protein complexes yield significant amounts of sequence-informative b/y-products, as CAD of protein complexes using other analyzers typically generate subunit separation products only (e.g., monomer and intact complex-minus-monomer products). Moreover, as indicated by other studies [40-42, 57], the sequence origin of the product ions

can be correlated to the outer surface regions of the complexes, suggesting that native tandem MS can be a potentially useful tool for probing the topology of protein assemblies.

## Supplementary Material

Refer to Web version on PubMed Central for supplementary material.

## ACKNOWLEDGMENTS

Support from the US National Institutes of Health (R01 GM103479 and S10 RR028893 to JAL) and the Development and Promotion of Science and Technology Talents Project (DPST), Royal Thai Government (to PW) are acknowledged.

## REFERENCES

1. van Duijn E. Current limitations in native mass spectrometry based structural biology. J. Am. Soc. Mass Spectrom. 2010; 21:971–978. [PubMed: 20116282]
2. Heck AJR. Native mass spectrometry: A bridge between interactomics and structural biology. Nat. Methods. 2008; 5:927–933. [PubMed: 18974734]
3. Sharon M. How far can we go with structural mass spectrometry of protein complexes? J. Am. Soc. Mass Spectrom. 2010; 21:487–500. [PubMed: 20116283]
4. Barrera NP, Robinson CV. Advances in the mass spectrometry of membrane proteins: From individual proteins to intact complexes. Annu. Rev. Biochem. 2011; 80:247–271. [PubMed: 21548785]
5. Zhou M, Robinson CV. When proteomics meets structural biology. Trends Biochem. Sci. 2010; 35:522–529. [PubMed: 20627589]
6. Benesch JLP, Robinson CV. Mass spectrometry of macromolecular assemblies: Preservation and dissociation. Curr. Opin. Struct. Biol. 2006; 16:245–251. [PubMed: 16563743]
7. Benesch JLP, Aquilina JA, Ruotolo BT, Sobott F, Robinson CV. Tandem mass spectrometry reveals the quaternary organization of macromolecular assemblies. Chem. Biol. 2006; 13:597–605. [PubMed: 16793517]
8. Benesch JLP, Sobott F, Robinson CV. Thermal dissociation of multimeric protein complexes by using nanoelectrospray mass spectrometry. Anal. Chem. 2003; 75:2208–2214. [PubMed: 12918957]
9. Painter AJ, Jaya N, Basha E, Vierling E, Robinson CV, Benesch JLP. Real-time monitoring of protein complexes reveals their quaternary organization and dynamics. Chem. Biol. 2008; 15:246–253. [PubMed: 18355724]
10. Lentze N, Aquilina JA, Lindbauer M, Robinson CV, Narberhaus F. Temperature and concentration-controlled dynamics of rhizobial small heat shock proteins. Eur. J. Biochem. 2004; 271:2494–2503. [PubMed: 15182365]
11. van Duijn E, Bakkes PJ, Heeren RMA, van den Heuvel RHH, van Heerikhuizen H, van der Vies SM, Heck AJR. Monitoring macromolecular complexes involved in the chaperonin-assisted protein folding cycle by mass spectrometry. Nat. Methods. 2005; 2:371–376. [PubMed: 15846365]
12. Snijder J, Rose RJ, Veesler D, Johnson JE, Heck AJR. Studying 18 mda virus assemblies with native mass spectrometry. Angew. Chem. Int. Ed. 2013; 52:4020–4023.
13. Van Berkel WJH, van den Heuvel RHH, Versluis C, Heck AJR. Detection of intact megadalton protein assemblies of vanillyl-alcohol oxidase by mass spectrometry. Protein Sci. 2000; 9:435–439. [PubMed: 10752605]
14. Uetrecht C, Rose RJ, van Duijn E, Lorenzen K, Heck AJR. Ion mobility mass spectrometry of proteins and protein assemblies. Chem. Soc. Rev. 2010; 39:1633–1655. [PubMed: 20419213]
15. Zhou M, Jones CM, Wysocki VH. Dissecting the large noncovalent protein complex groel with surface-induced dissociation and ion mobility–mass spectrometry. Anal. Chem. 2013; 85:8262–8267. [PubMed: 23855733]

16. Zhou M, Dagan S, Wysocki VH. Impact of charge state on gas-phase behaviors of noncovalent protein complexes in collision induced dissociation and surface induced dissociation. Analyst. 2013; 138:1353–1362. [PubMed: 23324896]
17. Zhou M, Dagan S, Wysocki VH. Protein subunits released by surface collisions of noncovalent complexes: Native like compact structures revealed by ion mobility mass spectrometry. Angew. Chem. Int. Ed. 2012; 51:4336–4339.
18. Rose RJ, Damoc E, Denisov E, Makarov A, Heck AJR. High-sensitivity orbitrap mass analysis of intact macromolecular assemblies. Nat. Methods. 2012; 9:1084–1086. [PubMed: 23064518]
19. Zubarev RA, Kelleher NL, McLafferty FW. Electron capture dissociation of multiply charged protein cations. A nonergodic process. J. Am. Chem. Soc. 1998; 120:3265–3266.
20. Mao Y, Valeja SG, Rouse JC, Hendrickson CL, Marshall AG. Top-down structural analysis of an intact monoclonal antibody by electron capture dissociation-fourier transform ion cyclotron resonance-mass spectrometry. Anal. Chem. 2013; 85:4239–4246. [PubMed: 23551206]
21. Li H, Lin T-Y, Van Orden SL, Zhao Y, Barrow MP, Pizarro AM, Qi Y, Sadler PJ, O'Connor PB. Use of top-down and bottom-up fourier transform ion cyclotron resonance mass spectrometry for mapping calmodulin sites modified by platinum anticancer drugs. Anal. Chem. 2011; 83:9507–9515. [PubMed: 22032417]
22. Ge Y, Rybakova IN, Xu Q, Moss RL. Top-down high-resolution mass spectrometry of cardiac myosin binding protein c revealed that truncation alters protein phosphorylation state. Proc. Natl. Acad. Sci. USA. 2009; 106:12658–12663. [PubMed: 19541641]
23. Breuker K, Jin M, Han X, Jiang H, McLafferty FW. Top-down identification and characterization of biomolecules by mass spectrometry. J. Am. Soc. Mass Spectrom. 2008; 19:1045–1053. [PubMed: 18571936]
24. Zhang H, Ge Y. Comprehensive analysis of protein modifications by top-down mass spectrometry. Circ. Cardiovasc. Genet. 2011; 4:711. [PubMed: 22187450]
25. Pesavento JJ, Kim Y-B, Taylor GK, Kelleher NL. Shotgun annotation of histone modifications: A new approach for streamlined characterization of proteins by top down mass spectrometry. J. Am. Chem. Soc. 2004; 126:3386–3387. [PubMed: 15025441]
26. Fridriksson EK, Beavil A, Holowka D, Gould HJ, Baird B, McLafferty FW. Heterogeneous glycosylation of immunoglobulin e constructs characterized by top-down high-resolution 2-D mass spectrometry. Biochemistry. 2000; 39:3369–3376. [PubMed: 10727230]
27. Kelleher NL, Taylor SV, Grannis D, Kinsland C, Chiu H-J, Begley TP, McLafferty FW. Efficient sequence analysis of the six gene products (7-74 kDa) from the escherichia coli thiamin biosynthetic operon by tandem high-resolution mass spectrometry. Protein Sci. 1998; 7:1796–1801. [PubMed: 10082377]
28. Ge Y, Lawhorn BG, ElNaggar M, Strauss E, Park J-H, Begley TP, McLafferty FW. Top down characterization of larger proteins (45 kDa) by electron capture dissociation mass spectrometry. J. Am. Chem. Soc. 2002; 124:672–678. [PubMed: 11804498]
29. Wood TD, Chen LH, Kelleher NL, Little DP, Kenyon GL, McLafferty FW. Direct sequence data from heterogeneous creatine kinase (43 kDa) by high-resolution tandem mass spectrometry. Biochemistry. 1995; 34:16251–16254. [PubMed: 8845349]
30. Han X, Jin M, Breuker K, McLafferty FW. Extending top-down mass spectrometry to proteins with masses greater than 200 kilodaltons. Science. 2006; 314:109–112. [PubMed: 17023655]
31. Breuker K, McLafferty FW. Stepwise evolution of protein native structure with electrospray into the gas phase, $10^{-12}$ to $10^{2}$ s. Proc. Natl. Acad. Sci. USA. 2008; 105:18145–18152. [PubMed: 19033474]
32. Schennach M, Breuker K. Proteins with highly similar native folds can show vastly dissimilar folding behavior when desolvated. Angew. Chem. Int. Ed. 2014; 53:164–168.
33. Breuker K, Brüschweiler S, Tollinger M. Electrostatic stabilization of a native protein structure in the gas phase. Angew. Chem. Int. Ed. 2011; 50:873–877.
34. Sze SK, Ge Y, Oh H, McLafferty FW. Top-down mass spectrometry of a 29-kDa protein for characterization of any posttranslational modification to within one residue. Proc. Natl. Acad. Sci. USA. 2002; 99:1774–1779. [PubMed: 11842225]

35. Yin S, Loo JA. Top-down mass spectrometry of supercharged native protein–ligand complexes. Int. J. Mass Spectrom. 2011; 300:118–122. [PubMed: 21499519]
36. Clarke D, Murray E, Hupp T, Mackay CL, Langridge-Smith PR. Mapping a noncovalent protein–peptide interface by top-down FTICR mass spectrometry using electron capture dissociation. J. Am. Soc. Mass Spectrom. 2011; 22:1432–1440. [PubMed: 21953198]
37. Yin S, Loo JA. Elucidating the site of protein-ATP binding by top-down mass spectrometry. J. Am. Soc. Mass Spectrom. 2010; 21:899–907. [PubMed: 20163968]
38. Xie Y, Zhang J, Yin S, Loo JA. Top-down ESI-ECD-FT-ICR mass spectrometry localizes noncovalent protein-ligand binding sites. J. Am. Chem. Soc. 2006; 128:14432–14433. [PubMed: 17090006]
39. Geels RBJ, van der Vies SM, Heck AJR, Heeren RMA. Electron capture dissociation as structural probe for noncovalent gas-phase protein assemblies. Anal. Chem. 2006; 78:7191–7196. [PubMed: 17037920]
40. Zhang H, Cui W, Wen J, Blankenship RE, Gross ML. Native electrospray and electron-capture dissociation FTICR mass spectrometry for top-down studies of protein assemblies. Anal. Chem. 2011; 83:5598–5606. [PubMed: 21612283]
41. Zhang H, Cui W, Wen J, Blankenship R, Gross M. Native electrospray and electron-capture dissociation in FTICR mass spectrometry provide top-down sequencing of a protein component in an intact protein assembly. J. Am. Soc. Mass Spectrom. 2010; 21:1966–1968. [PubMed: 20843701]
42. Li H, Wolff JJ, Van Orden SL, Loo JA. Native top-down electrospray ionization-mass spectrometry of 158 kDa protein complex by high-resolution fourier transform ion cyclotron resonance mass spectrometry. Anal. Chem. 2014; 86:317–320. [PubMed: 24313806]
43. Loo JA, Udseth HR, Smith RD, Futrell JH. Collisional effects on the charge distribution of ions from large molecules, formed by electrospray-ionization mass spectrometry. Rapid Commun. Mass Spectrom. 1988; 2:207–210.
44. Loo JA, Edmonds CG, Smith RD. Tandem mass spectrometry of very large molecules: Serum albumin sequence information from multiply charged ions formed by electrospray ionization. Anal. Chem. 1991; 63:2488–2499. [PubMed: 1763807]
45. Theorell, H. Structural and Functional Relationships between Isoenzymes of Horse LADH.. In: Sund, H., editor. Pyridine Nucleotide-Dependent Dehydrogenases. Springer-Verlag; Berlin: 1970. p. 121-128.
46. Adolph H-W, Zwart P, Meijers R, Hubatsch I, Kiefer M, Lamzin V, Cedergren-Zeppezauer E. Structural basis for substrate specificity differences of horse liver alcohol dehydrogenase isozymes. Biochemistry. 2000; 39:12885–12897. [PubMed: 11041853]
47. Gardner MW, Brodbelt JS. Impact of proline and aspartic acid residues on the dissociation of intermolecularly crosslinked peptides. J. Am. Soc. Mass Spectrom. 2008; 19:344–357. [PubMed: 18083526]
48. Tsaprailis G, Somogyi Á, Nikolaev EN, Wysocki VH. Refining the model for selective cleavage at acidic residues in arginine-containing protonated peptides. Int. J. Mass Spectrom. 2000; 195–196:467–479.
49. Yu W, Vath JE, Huberty MC, Martin SA. Identification of the facile gas-phase cleavage of the Asp-Pro and Asp-Xxx peptide bonds in matrix-assisted laser desorption time-of-flight mass spectrometry. Anal. Chem. 1993; 65:3015–3023. [PubMed: 8256865]
50. Jörnvall H. The primary structure of yeast alcohol dehydrogenase. Eur. J. Biochem. 1977; 72:425–442. [PubMed: 320000]
51. Savitski MM, Nielsen ML, Zubarev RA. Side-chain losses in electron capture dissociation to improve peptide identification. Anal. Chem. 2007; 79:2296–2302. [PubMed: 17274597]
52. Han H, Xia Y, McLuckey SA. Ion trap collisional activation of c and z• ions formed via gas-phase ion/ion electron-transfer dissociation. J. Proteome Res. 2007; 6:3062–3069. [PubMed: 17608403]
53. Dalziel K. The purification of nicotinamide adenine dinucleotide and the kinetic effects of nucleotide impurities. J. Biol. Chem. 1963; 238:1538–1543. [PubMed: 14024804]

54. Dickenson CJ, Dickinson FM. A study of the pH- and temperature-dependence of the reactions of yeast alcohol dehydrogenase with ethanol, acetaldehyde and butyraldehyde as substrates. Biochem. J. 1975; 147:303–311. [PubMed: 241323]

55. Al-Karadaghi S, Cedergren-Zeppezauer ES, Hovmoller S, Petratos K, Terry H, Wilson KS. Refined crystal structure of liver alcohol dehydrogenase-nadh complex at 1.8 Å resolution. Acta Crystallogr., Sect D: Biol. Crystallogr. 1994; 50:793–807. [PubMed: 15299346]

56. Plapp BV, Savarimuthu BR, Ramaswamy S. Asymmetry in a structure of yeast alcohol dehydrogenase. DOI:10.2210/pdb2hcy/pdb (To be published).

57. Cui W, Rohrs HW, Gross ML. Top-down mass spectrometry: Recent developments, applications and perspectives. Analyst. 2011; 136:3854–3864. [PubMed: 21826297]

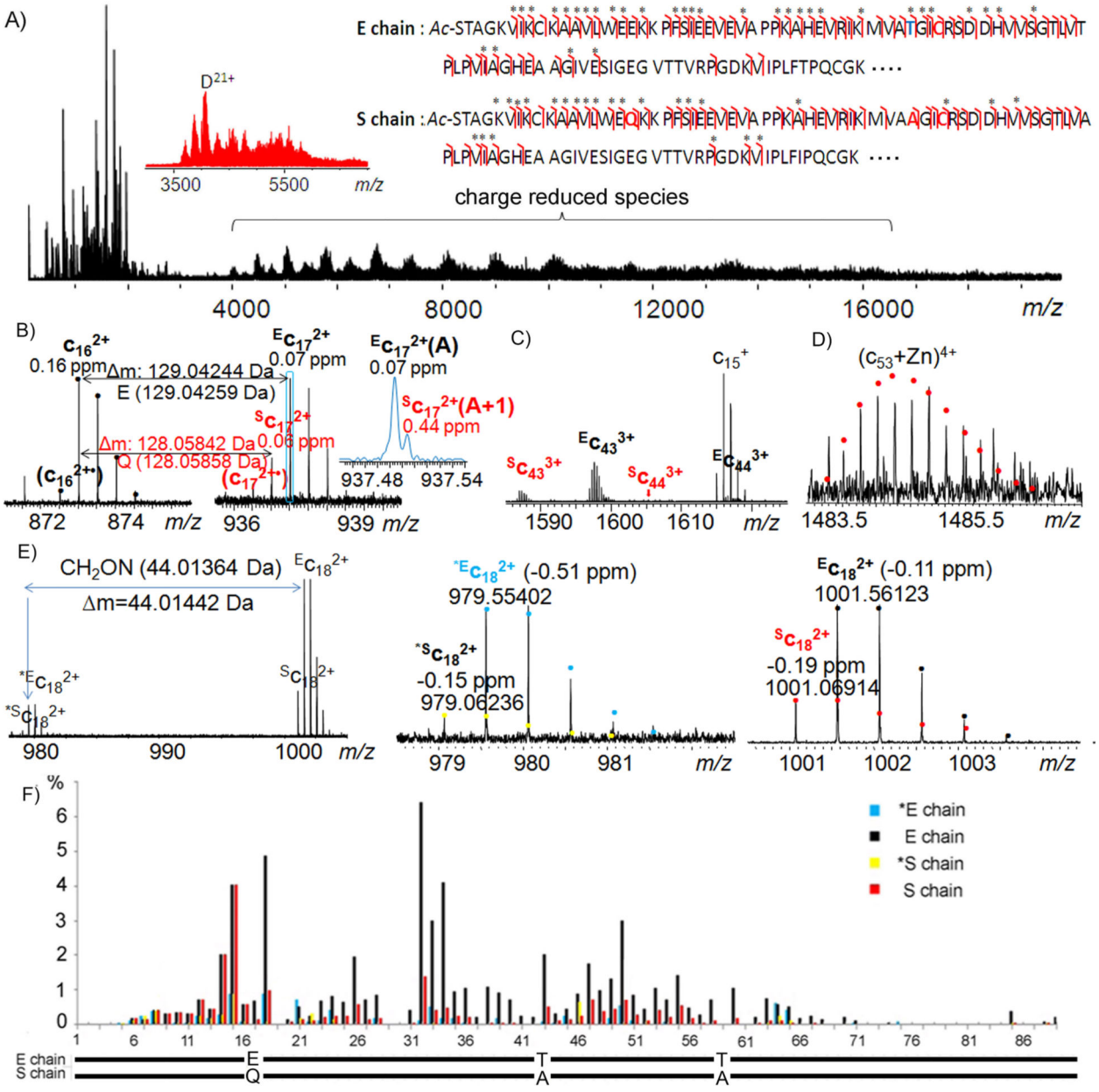


**Figure 1.**

(A) Native top-down ECD of hADH dimer. The insets show the full MS spectrum of hADH dimer at *m/z* 3500–4500 and the ECD fragmentation map. The sites with the -44.01364 Da mass shifts are indicated with "*". (B) and (C) Subunit variants differentiation, (D) zinc binding site, (E) putative PTM, and (F) normalized abundance of native top-down ECD fragment ions of hADH dimer.

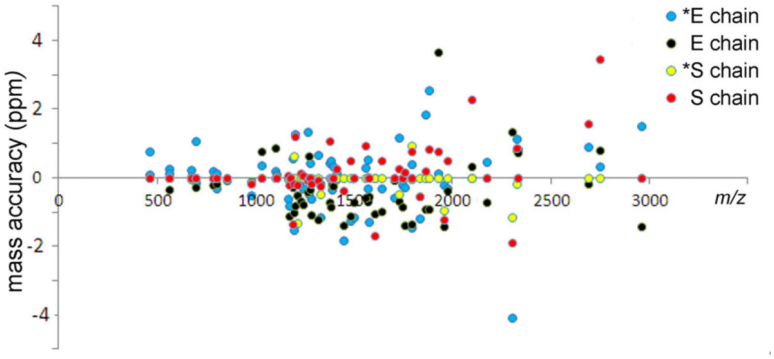


**Figure 2.**

Mass accuracy of product ions from native top-down ECD of hADH. *E chain in blue, E chain in black, *S chain in yellow, and S chain in red.

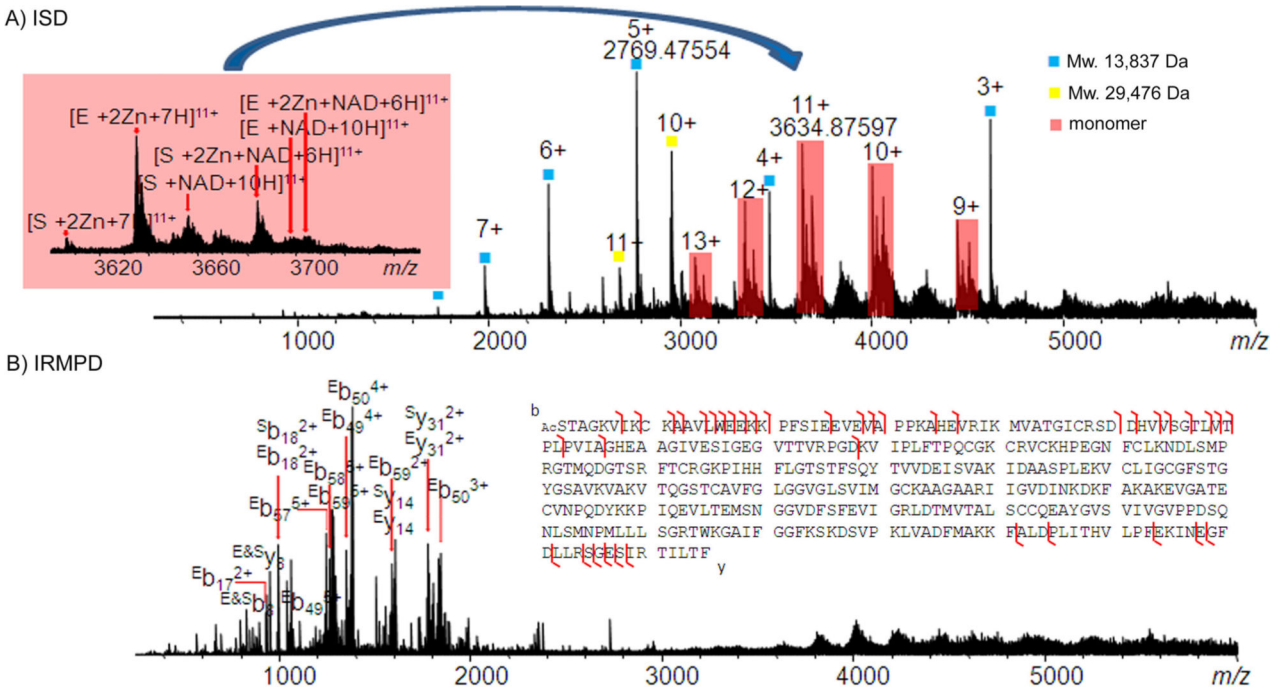


**Figure 3.**

Native top-down (A) ISD and (B) IRMPD mass spectra of hADH. The inset of Figure 3A shows the 11+ charge state of hADH subunits with zinc and $NAD^+$ binding. The inset of Figure 3B shows the top-down IRMPD fragmentation scheme.

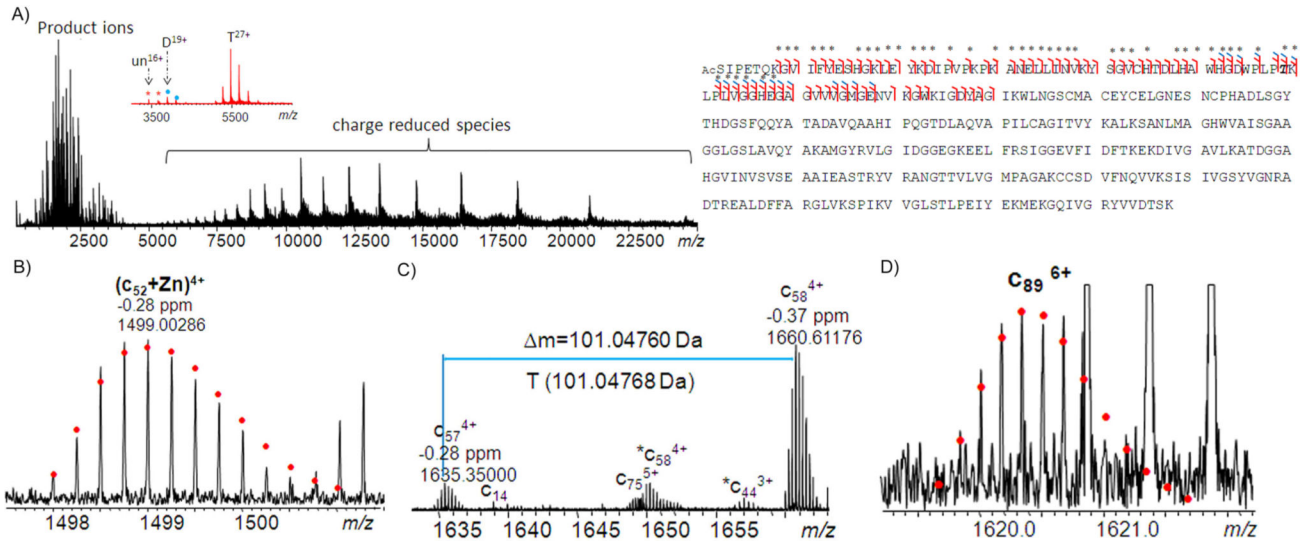


**Figure 4.**

(A) Native top-down ECD of yADH and the fragmentation scheme. The inset shows the full MS spectrum of yADH tetramer centered at *m/z* 5000, along with ions for the ADH dimer (at *m/z* 3600~3700) and an unknown 58 kDa protein (at *m/z* 3400~3600). (B) Zinc binding ion, $c_{52}$, (C) site mutation V58T, and (D) $c_{89}$ ions.

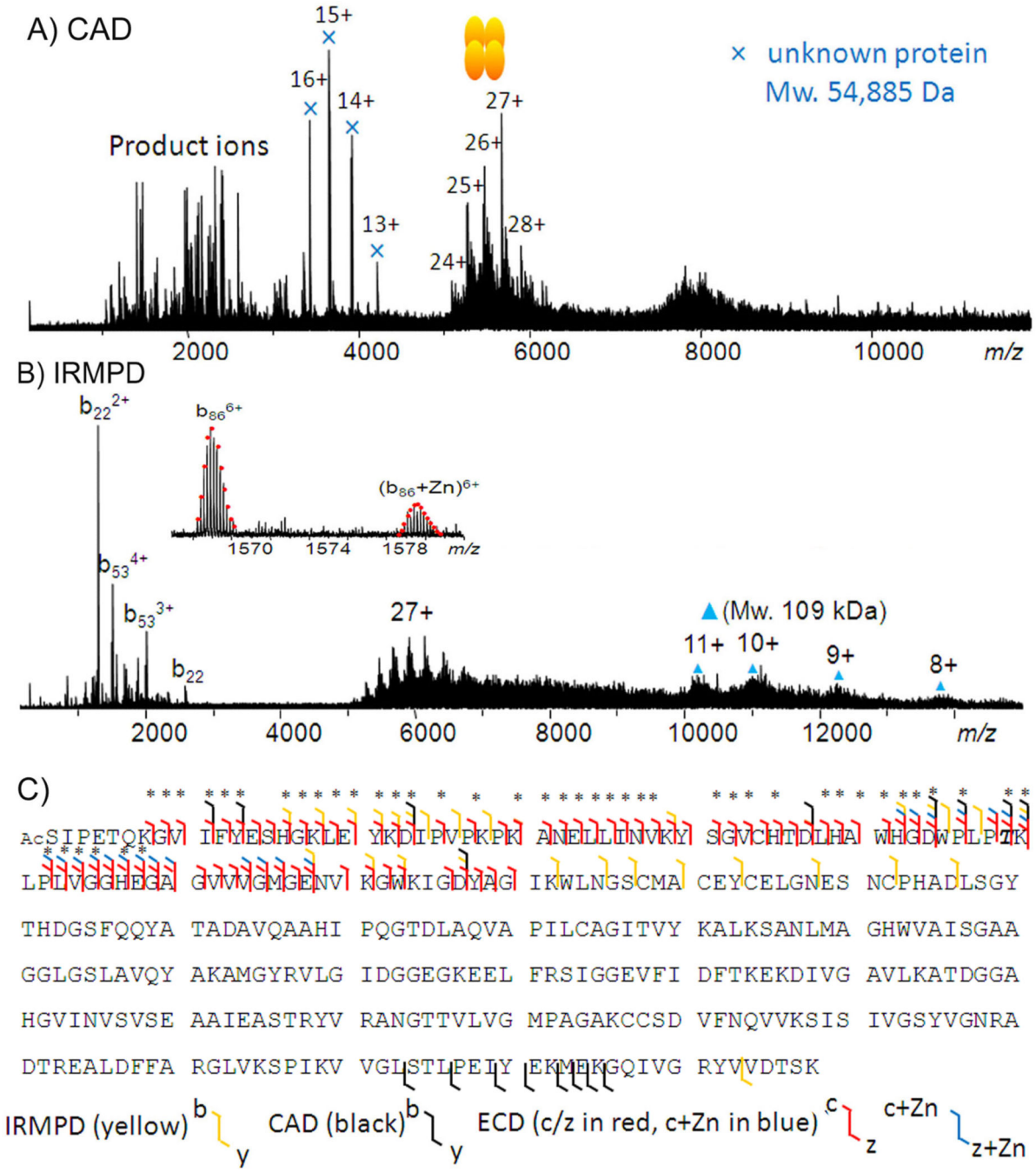


**Figure 5.**

Native top-down (A) CAD and (B) IRMPD of yADH. The inset on the left-hand side of Figure 5B shows the observation of zinc binding ion $b_{86}$, and the inset on the right-hand side shows the top-down IRMPD fragmentation scheme of yADH.

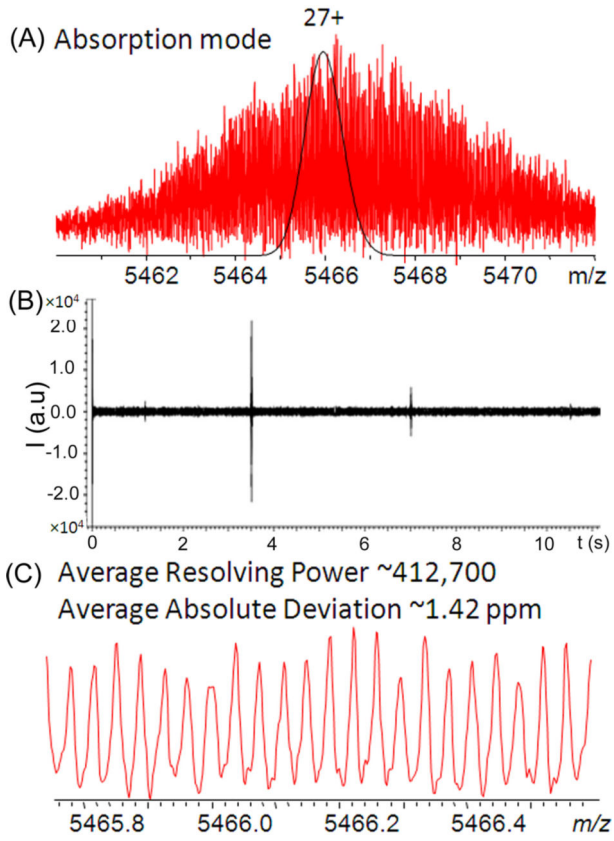


**Figure 6.**

A) The isotopic resolved 27+ mass spectrum of yADH tetramer in absorption mode, with the simulated black peak outlining the $[(M+2Zn)_4+19H]^{27+}$ peak position; B) transient recorded for the 27+ ions of yADH; C) the expanded spectrum of the $[(C_{1640}H_{2576}N_{440}O_{491}S_{14}+2Zn)_4+19H]^{27+}$ ions of yADH.